5*d* electron delocalization of Ce^{3+} and Pr^{3+} in Y_2SiO_5 and Lu_2SiO_5

E. van der Kolk, P. Dorenbos, and C. W. E. van Eijk
Faculty of Applied Sciences, Delft University of Technology, Mekelweg 15, 2629 JB Delft, The Netherlands

S. A. Basun
A.F. Ioffe Physico-Technical Institute, St. Petersburg, Russia

G. F. Imbusch
Department of Physics, National University of Ireland, Galway, Ireland

W. M. Yen
Department of Physics and Astronomy, University of Georgia, Athens Georgia 30602, USA
(Received 24 December 2004; published 29 April 2005)

The energies of the 5*d* excited states of Ce^{3+} and Pr^{3+} impurities relative to the conduction band of the insulators Y_2SiO_5 and Lu_2SiO_5 were investigated through a temperature and spectrally resolved photoconductivity study. The effective ionization barrier of Pr^{3+} from the 5*d* state to the conduction band is found to be 0.15 eV smaller than that of Ce^{3+} in both Y_2SiO_5 and Lu_2SiO_5. The difference is explained by a model, represented by rate equations, that takes into account interconfigurational $4f5d \rightarrow 4f^2$ relaxation for Pr^{3+}, a process that is absent for Ce^{3+}.

DOI: 10.1103/PhysRevB.71.165120 PACS number(s): 78.55.Hx, 71.55.−i, 72.80.Sk

I. INTRODUCTION

The energies of the ground and excited states of lanthanide impurities in insulators relative to the intrinsic bands of the crystalline host can greatly influence the efficiency of luminescent materials such as lasers, phosphors, and scintillators.[1,2] A reliable model predicting the absolute locations of these levels will be extremely useful but does not exist at the moment. As a starting point the relative positions of lanthanide 4*f* and 5*d* states within the bandgap has recently been established. On the basis of ultraviolet photoelectron spectroscopy (UPS) Thiel *et al.*[3,4] determined the ground state location of trivalent lanthanides in various compounds and proposed a two parameter empirical model to describe it. One parameter represents the binding energy shift experienced by all lanthanides and another parameter represents an ion size dependent shift. Combining this model with an empirical model on $4f^{n-1}5d^1$ transition energies by Dorenbos,[5] Thiel *et al.* proposed a simple three parameter model that describes both the $4f^n$ ground state and the $4f^{n-1}5d^1$ excited state. An application to $Y_3Al_5O_{12}$ revealed that the energy of the lowest 5*d* state decreases by about 1 eV in going through the lanthanide series from Ce^{3+} to Lu^{3+}. In addition it was found that the 5*d* state of Pr^{3+} is about 0.7 eV farther below the conduction band (CB) than the 5*d* state of Ce^{3+}. A major drawback of using UPS or XPS is the possible presence of a large systematic error in the determination of binding energies and the need to study high doping concentrations.

A different approach was followed by Dorenbos[6–8] to determine the level locations for the divalent lanthanides. By using the energy of charge transfer (CT) from the valence band to a trivalent lanthanide, the ground state location of the corresponding divalent lanthanide is obtained. XPS and UPS information on trivalent lanthanides is sparsely available but there exists a huge amount of spectroscopic information on CT energies. By collecting and analyzing these CT data, a similar empirical three parameter model was developed for divalent lanthanides. It was found, for example, that the lowest 5*d* state of Yb^{2+} relative to the bottom of the conduction band is always about 0.5 eV higher than that of Eu^{2+}. By means of extrapolation, the 5*d* level position of Ce^{2+} to Eu^{2+} was found to be almost constant (within 0.1 eV). By analogy with the divalent lanthanides, a method was proposed to construct the energy levels of the trivalent lanthanides also. Once the location of the lowest 5*d* state of Ce^{3+} has been determined together with the energy difference between 4*f* and 5*d*, the levels of all trivalent lanthanides can be constructed. Although the method of construction was made plausible, there has not yet been direct experimental verification for the predicted almost constant value of the lowest 5*d* level positions for the trivalent lanthanides from Ce to Eu.

In order to observe small differences between different lanthanide ions in the same host, energy level placement should have a precision of typically better than 0.1 eV. In some cases[10,9] such precision can be achieved by exploring the temperature dependence of photocurrent (PC) excitation spectra. The thermally stimulated ionization efficiency from the 5*d* states to the CB can be used to measure the ionization energy barrier (and therewith derive a value for the lowest energy 5*d* level position) with a precision considerably better than 0.1 eV. In this work we have used this method to detect differences between the lowest 5*d* level positions of Ce^{3+} and Pr^{3+} in Lu_2SiO_5 (LSO) and Y_2SiO_5 (YSO).

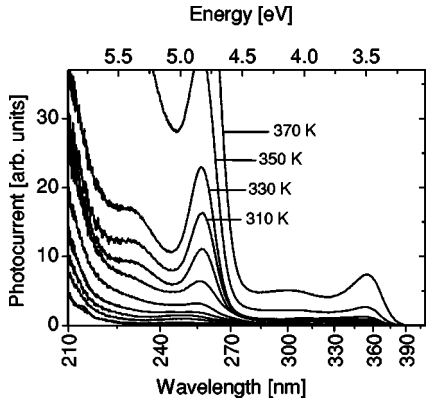

FIG. 1. Photocurrent excitation spectra of $Y_2SiO_5:Pr^{3+}$ between 110 and 370 K with incremental steps of 20 K.

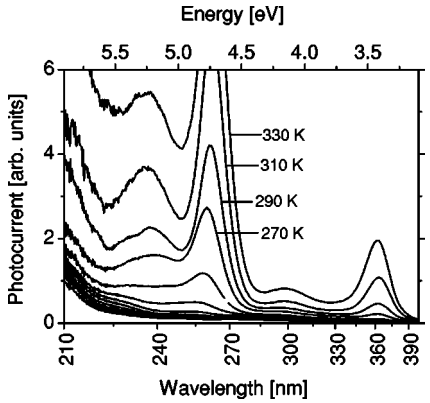

FIG. 2. Photocurrent excitation spectra of $Lu_2SiO_5:Pr^{3+}$ between 150 and 330 K with incremental steps of 20 K.

II. EXPERIMENT AND CRYSTALS

The experimental method used to record the temperature dependence of photocurrent excitation spectra was described before.[10,12] The crystal growth method used to obtain the 0.8% Pr^{3+} doped Y_2SiO_5 (YSO) and Lu_2SiO_5 (LSO) single crystals, was described earlier by one of us.[13] The crystal structures of LSO and YSO are the same. The interionic distances for YSO are slightly larger compared to those of LSO due to the few % larger ionic radius of Y^{3+} compared to Lu^{3+}. From optical and luminescence data on the Pr^{3+} doped crystals, it could be concluded that Ce^{3+} centers are unintentionally present in our crystals.

In LSO (or YSO) Pr^{3+} and Ce^{3+} ions occupy both the two crystallographically different Lu (or Y) sites called Lu_1 and Lu_2.[15] In an earlier PC study of $LSO:Ce^{3+}$ (Ref. 10) it was concluded that Ce^{3+} ions occupying both the two Lu sites undergo ionization and are involved in the photocurrent process. Recent PC studies by one of us, on $LSO:Ce^{3+}$ crystals with different optical densities, have revealed however that the doublet structure of the lowest energy 5*d* state of Ce^{3+} as observed in PC spectra,[10] is the result of a saturation effect (that will not be discussed in this work), rather than due to the presence of Ce^{3+} ions on two different crystallographical sites. The experimental photocurrent data that will be presented in this work show no doublet structure in the lowest energy 5*d* band of Ce^{3+} or Pr^{3+}. Given these contradicting experimental results, the assignment of the photocurrent to both sites or to either of the two particular sites remains uncertain.

III. EXPERIMENTAL RESULTS

Figure 1 shows the temperature dependence of the photocurrent excitation spectra of Pr^{3+} doped YSO between 150 and 370 K and 210 and 425 nm. At temperatures below 200 K, a structureless photocurrent background signal is observed that becomes increasingly intense towards higher energy and starts to rise strongly towards the band to band transition of YSO. At about 250 K, a weak feature becomes visible at 260 nm that is assigned to the lowest energy $4f^2 \rightarrow 4f5d$ transition on the Pr^{3+} ion. Since this is a localized transition, the observed photocurrent can only be the result of a subsequent delocalization process after optical excitation. Because of the strong temperature dependence, and in analogy with previous PC studies[10,11] on $LSO:Ce^{3+}$, the delocalization is ascribed to a thermally stimulated ionization process of optically excited Pr^{3+} ions from the lowest energy 5*d* state to the conduction band. The intensity of this band continues to rise exponentially with temperature. At about 290 K, a second feature at longer wavelength (360 nm) appears that is assigned to the $4f \rightarrow 5d$ transition on the Ce^{3+} ions that are present unintentionally in the crystal. The assignment to 5*d* excited states of Ce^{3+} and Pr^{3+} is based on previously published luminescence excitation and absorption data on these ions in Y_2SiO_5.[13–16]

Figure 2 contains the same type of experimental data as shown in Fig. 1, but now for $LSO:Pr^{3+}$ instead of $YSO:Pr^{3+}$. Also, in LSO a strong temperature-dependent photocurrent excitation band can be observed at around 260 nm. The energy of this band matches the energy of the transition to the lowest energy $4f5d$ state of Pr^{3+}, as observed by us in luminescence excitation spectra (unpublished). Also, in this crystal unintentional Ce^{3+} impurities cause a photocurrent excitation band. At 363 nm the Ce^{3+} lowest energy 5*d* state is detected in the photocurrent excitation spectra.

By determining the temperature-dependent intensity of the photocurrent associated with the lowest energy 5*d* states of Ce^{3+} and Pr^{3+}, as observed in the PC spectra presented in Figs. 1 and 2, an Arrhenius diagram can be constructed. Figure 3 contains such intensity data for Pr^{3+} (open symbols) and Ce^{3+} (filled symbols) in both LSO (squares) and YSO (circles). The straight line fits show that, in each compound, the temperature dependence is dominated by a single energy barrier. If we interpret this energy barrier as the energy separation between the lowest 5*d* state and the bottom of the CB, then we find energy separations of 0.44 eV and 0.41 eV for Ce^{3+} in YSO and LSO, respectively. For Pr^{3+}, the energies are smaller: 0.29 eV and 0.25 eV for YSO and LSO, respectively. From this it is tempting to conclude that the lowest energy 5*d* states of Pr^{3+} are about 0.15 eV closer to the CB than the lowest energy 5*d* states of Ce^{3+} in these materials. In the next section we show that, in the case of the Pr^{3+} ions, the Arrhenius plot of pho-

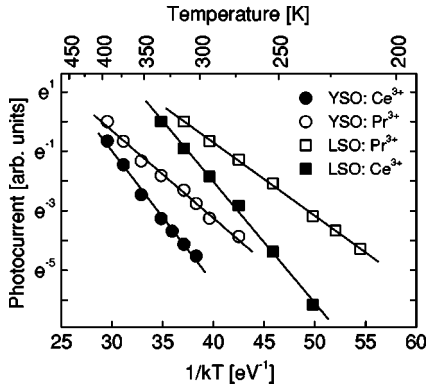

FIG. 3. Arrhenius plot of the photocurrent intensity of Pr^{3+} (open symbols) and Ce^{3+} (filled symbols) in both LSO (squares) and YSO (circles) upon excitation into the lowest energy Ce^{3+} or Pr^{3+} 5*d* states. Solid lines represent fits to the data.

tocurrent against temperature does not admit such a simple interpretation, and that the effective ionization barrier obtained from the Arrhenius plot is smaller than the energy separation between the lowest 5*d* states of Pr^{3+} and the bottom of the CB.

IV. ANALYSIS OF MEASUREMENTS

In this section we analyze the 0.15 eV difference between the ionization barriers of Ce^{3+} and Pr^{3+}, as derived from the photoconductivity measurements. We consider how the photoconductivity measurements, in the case of Pr^{3+}, are affected by a possible temperature-dependent energy transfer from the lowest energy $4f5d$ state to the ^3P and ^1I states of the $4f^2$ configuration. Such an intersystem crossing is commonly observed for Pr^{3+} in compounds for which the $4f5d$ configuration is not located at too high energy above levels of the $4f^2$ configuration. Indeed, in LSO and in YSO, emission from the $^3P_{0,1}$ states can be observed when the lowest energy $4f5d$ state is excited. This intersystem crossing can be represented by the configuration coordinate diagram shown in Fig. 4. After optical excitation from the $4f^2[^3H_4]$ ground state of Pr^{3+} into point *a* on the parabola corresponding to the lowest energy $4f5d$ state, the

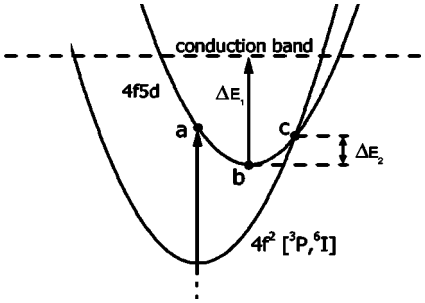

FIG. 4. Higher energy part of the single coordinate configuration diagram of Pr^{3+} with the parabolas representing the $4f^2$ and the $4f5d$ configurations. ΔE_1 is the thermal ionization energy barrier. ΔE_2 is the energy barrier for $4f5d \rightarrow 4f^2$ interconfigurational relaxation.

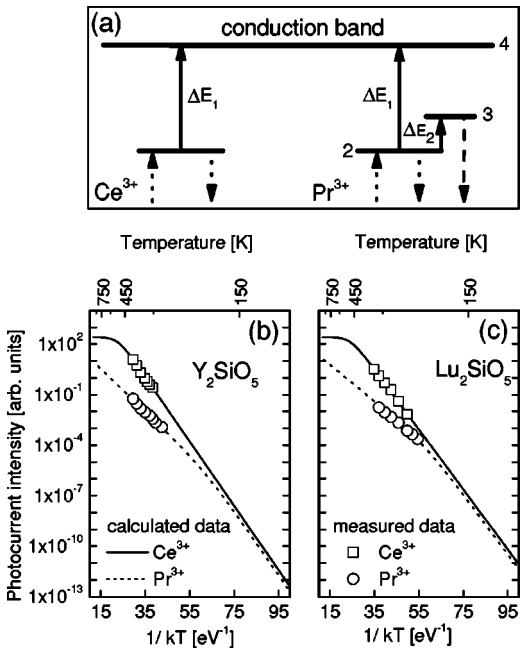

FIG. 5. (a) Energy level diagram of the lowest energy 5*d* state of Ce^{3+} (left) and Pr^{3+} (right) below the CB. Solid arrows indicate thermal ionization. The dotted arrows indicate $4f^2 \rightarrow 4f5d$ pumping and $4f5d \rightarrow 4f^2$ emission. The $4f^2 \rightarrow 4f^2$ transition is also indicated (dashed). (b) and (c) Calculated photocurrent (proportional to the number of electrons in the CB) of Ce^{3+} (solid lines) and Pr^{3+} (dotted lines), upon excitation into the lowest energy 5*d* state, represented in an Arrhenius diagram for both Y_2SiO_5 (b) and Lu_2SiO_5 (c). The symbols are the measured photocurrent data that was presented in Fig. 3 multiplied by a constant.

system will relax via lattice relaxation to the lowest energy point *b*. From this point three processes are possible. First, emission can take place to states of the $4f^2$ configuration. Second, thermal ionization to the bottom of the conduction band is possible with an energy barrier of ΔE_1. Third, nonradiative relaxation via the crossover point between the two parabolas (point *c*) is possible. The last process has an energy barrier equal to ΔE_2 and will affect the population of excited Pr^{3+} ions. As a result it lowers the ionization efficiency and consequently the slope in the Arrhenius diagram that no longer represents the position of the Pr^{3+} 5*d* position relative to the conduction band.

In the following, the efficiency and the temperature dependence of the thermal ionization process of Ce^{3+} and Pr^{3+} is calculated by solving the rate equations corresponding to the level schemes shown in Fig. 5(a). In case of Ce^{3+} (left picture) the calculations involve excitation and emission involving the lowest energy 5*d* state as well as thermal ionization into the conduction band and Ce^{4+}+electron nonradiative recombination (not shown). For Pr^{3+} (the right picture in Fig. 5(a)) also the thermally stimulated transfer from the $4f5d$ state to the $4f^2$ state and the subsequent $4f^2[^3P_{0,1}] \rightarrow 4f^2$ emission is considered.

The rate equations for the Pr^{3+} doped system are as follows:

$$n_1' = -c_{12}n_1 + c_{21}n_2 + c_{31}n_3 + c_{41}n_4,$$

$$n_2' = c_{12}n_1 - (c_{21} + c_{23} + c_{24})n_2,$$

$$n_3' = c_{23}n_2 - c_{31}n_3,$$

$$n_4' = -c_{41}n_4 + c_{24}n_2, \quad (1)$$

in which n_1 is the fraction of Pr^{3+} ions in the ground state and n_2 through n_4 are the fractions of Pr^{3+} ions in the states indicated in the right part of Fig 5(a), in order of icreasing energy. $n' \equiv dn/dt$. The constant coefficients c_{ij} (s^{-1}) are given by $c_{12}=10^{-5}$ (Pr^{3+} excitation rate); $c_{21}=10^8$ (Pr^{3+} $4f5d \rightarrow 4f^2$ decay rate); $c_{31}=10^5$ (Pr^{3+} $4f^2[^3P_{0,1}] \rightarrow 4f^2$ decay rate); $c_{23}=f_0e^{-\Delta E_2/kT}$ (thermally stimulated intersystem crossing rate); $c_{24}=f_0e^{-\Delta E_1/kT}$ (thermally stimulated ionization rate); $c_{41}=10^{10}$ (electron- Pr^{4+} recombination rate, $\tau=0.1$ ns). f_0 and k are the frequency factor or attempt frequency and Bolzmann's constant, respectively. ΔE_1 and ΔE_2 are indicated in Fig. 5(a). c_{12} is equal to the product of the photon flux ($\approx 10^{12}$ s^{-1} cm^{-2}) and the absorption cross section ($\approx 10^{-16}$ cm^2). c_{41} is determined by the lifetime of the electrons in the CB that can only be estimated. Note, however, that while c_{41} and c_{12} strongly affect the magnitude of the photocurrent intensity, they do not affect the temperature dependence. Possible errors in their values, therefore, have no consequences for the discussion below. Steady state thermal ionization rates as a function of temperature were calculated from these rate equations in the same way as was done in Ref. 9. In Figs. 5(b) and 5(c) the calculated steady state photocurrent, which is proportional to the number of electrons in the CB, for Ce^{3+} (solid line) and Pr^{3+} (dotted line) in both YSO (Fig. 5(b)) and LSO (Fig. 5(c)) are compared with experimental data (symbols) from Fig. 3.

The temperature dependence of Ce^{3+} is controlled by a single exponential with ΔE_1 equal to the energy separation between the Ce^{3+} 5*d* state and the CB bottom. Only at high temperature the photocurrent starts to saturate when the ionization rate becomes equal to the optical excitation rate. This interpretation of the calculated Ce^{3+} data is the same as that for $GdAlO_3$ described in Ref. 9. The experimental data for Ce^{3+} match well with the calculations when the earlier obtained ΔE_1 values of 0.44 and 0.41 eV are used for YSO and LSO, respectively.

The calculations for Pr^{3+} (dotted lines) are less straightforward. At low temperature the calculated Pr^{3+} photocurrent appears to have the same temperature dependence as Ce^{3+} when the same ΔE_1 values are chosen. Above about 225 K the slope in the Arrhenius diagram decreases and matches the experimental data when a value of $\Delta E_2=0.15$ and 0.16 eV is chosen for YSO and LSO, respectively. The measured slopes (0.29 and 0.25 eV for YSO and LSO, respectively) appear to be equal to $\Delta E_1 - \Delta E_2$. Below we show that this is not merely a numerical coincidence but that there is a clear reason.

Since all experimental data were obtained under steady state conditions, for which $dn/dt \equiv 0$, the following formula for n_4 (proportional to the PC intensity) can be derived from the rate equation

$$n_4 = n_1 \frac{c_{12}}{(c_{21} + c_{23} + c_{24})} \frac{c_{24}}{c_{41}}. \quad (2)$$

Since the experimental pumping rate (c_{12}) is very small, only a negligible fraction of the Pr^{3+} ions are raised to the excited state and n_1 can be considered as constant. Furthermore, using the values for f_0, ΔE_1 and ΔE_2, obtained from the numerical analysis above, we find that c_{24} is small compared with c_{23} for the whole temperature region of interest. Hence, c_{24} can be ignored in the denominator. The temperature dependence of n_4 is contained in the terms $c_{23}=f_0e^{-\Delta E_2/kT}$ and $c_{24}=f_0e^{-\Delta E_1/kT}$ only. c_{12} and c_{41} are constants that can be ignored when considering temperature dependence, so that the temperature dependence of n_4 is given by the factor $c_{24}/(c_{21}+c_{23})$.

Below about 150 K, c_{21} is sufficiently greater than c_{23} so that c_{23} can be ignored. The temperature dependence is then given by c_{24} only, which varies as $e^{-\Delta E_1/kT}$. Indeed, as observed in Figs. 5(a) and 5(b), the photocurrent of Pr^{3+} is controlled by an activation energy equal to the separation between the lowest energy 5*d* state and the bottom of the conduction band (ΔE_1). From 250 K upwards c_{23} is the larger term in the denominator and c_{21} can be ignored. In that case the temperature dependence of n_4 is given by the factor

$$\frac{c_{24}}{c_{23}} = e^{-(\Delta E_1 - \Delta E_2)/kT}. \quad (3)$$

Hence the measured ionization barrier no longer represents the separation between the lowest energy 5*d* state and the bottom of the conduction band (ΔE_1) but is lowered to an effective ionization barrier ($\Delta E_1 - \Delta E_2$) by an amount equal to the barrier for intersystem crossing (ΔE_2).

In the analysis above we have used, for simplicity, the same pre-exponential factor (f_0) for ionization and interconfigurational relaxation. Since the two processes are quite different in nature the corresponding frequency factors, defined as f_0^1 and f_0^2 respectively, may differ considerably. Below it will be shown that the analysis does not at all depend on the pre-exponential factors being equal, and is not very sensitive to the value chosen for f_0.

If we return to formula 2, and drop the c_{23} term, the formula can be applied to the Ce data. As long as c_{24} is smaller than c_{21}, the Arrhenius plot is linear, but turns over to a constant value when c_{24} becomes much bigger than c_{21}, as the calculated curves in Fig. 5(b) and 5(c) show. The turnover, where $c_{21} \approx c_{24}$, does not seem to be happening in the temperature region of the experiments. This should allow a limitation to be estimated for f_0^1 since the value of c_{21} is reasonably well known. Let us assume that the turnover happens just at the highest temperature that was reached (390 K) (limiting ourself to the YSO data); it can be expected that at this temperature $c_{21} \approx c_{24}$, or

$$f_0^1 \approx c_{21}e^{\Delta E_1/kT}. \quad (4)$$

Taking $c_{21}=10^8$, $\Delta E_1=0.44$ eV, and $T=390$ K, this gives $f_0^1 \approx 5 \times 10^{13}$. This puts an upper limit to the value of f_0^1.

In case of the Pr data the measured slope of 0.29 eV $(\Delta E_1 - \Delta E_2)$ was explained successfully by formula 2 for n_4 with the provision that $c_{24} < c_{23}$. Looking at the denominator in the equation for n_4, one can see that if $c_{23} \approx c_{24}$ in the temperature range of the experiments, then the Arrhenius plot will show a deviation from a straight line. Taking $1/kT = 35$ (around the middle of the experimental temperature range), $c_{23} \approx c_{24}$ gives

$$f_0^1 e^{-\Delta E_1/kT} \approx f_0^2 e^{-\Delta E_2/kT} \tag{5}$$

or

$$\frac{f_0^1}{f_0^2} \approx e^{(\Delta E_1 - \Delta E_2)/kT} \approx 10^4. \tag{6}$$

Although the method used to obtain this number is rather crude, it seems that the requirement that the pre-exponential factors have the same value is not necessary, only mathematically convenient. All that is needed to get a linear slope (of 0.29 eV) is that c_{23} be larger than c_{24} (and larger than c_{21}), and this only requires that f_0^1 be no more than about four orders of magnitude greater than f_0^2.

Looking once more at the Pr data, a kink between the two linear regions shows up in the calculated curves [see Figs. 5(b) and 5(c)]. If one assumes that the c_{23} process is faster than the c_{24} process (reasonable in view of the above argument) then the kink occurs when $c_{21} \approx c_{23}$, that is, when $f_0^2 = c_{21}(\Delta E_2/kT)$. All we know from the measurement is that the kink occurs at a lower temperature than that of the experiments. For YSO it could have occurred just below the lowest measured temperature for which $1/kT \approx 43$. Taking $c_{21} = 10^8$, and $\Delta E_2 = 0.18$, this gives $f_0^2 \approx 10^{11}$, giving a lower limit for f_0^2.

V. DISCUSSION AND CONCLUSIONS

The 0.41 eV found for LSO:Ce^{3+} in this work is smaller than the value of 0.45 ± 0.02 eV found in Ref. 10. In that respect we wish to note that the error in the Ce^{3+} data found in this work is larger ($\pm 0.03 - 0.04$ eV) due to the poorly defined background and the low concentration of Ce^{3+} that was present unintentionally in our samples. Although the values remain within the error margins it remains to be investigated how concentration affects the measured energy barrier. The 0.44 eV found for YSO:Ce^{3+} in this work is smaller than the value of 0.49 eV found by Choi *et al.*[14] In that work, however, the PC spectra were interpreted in a different way. The onset at low temperature of the PC spectrum was interpreted as the energy separation from the Ce^{3+} ground state to the CB. It is in our opinion more likely that this onset should be interpreted as the onset of excitation into the second lowest energy 5*d* state of Pr^{3+} located in the CB that is followed by delocalization of the 5*d* electron.

The physical origin of the position of energy levels of lanthanide ions along the lanthanide series relative to the CB was first discussed by Pedrini *et al.*[17] He related differences in ionization energy between different lanthanide ions (in the same compound) to the variation in electrostatic energy (Madelung energy) at the lanthanide site. When moving through the lathanide series $(Ce^{3+}, Pr^{3+}, Nd^{3+}, \ldots, Yb^{3+})$ the lanthanide contraction induces lattice relaxation that raises the Madelung energy term. As a result the 5*d* energy levels will move to higher energy with respect to the host bands. When a simple point charge electrostatic model is used[1,6] the difference in ionization energy between Ce^{3+} and Pr^{3+} as a result of Madelung energy only can be calculated to be about 0.2 eV. This value comes close to the experimentally measured difference of 0.15 eV (this work). There are, however, other terms besides the Madelung energy term that cause the ionization energy to change along the lanthanide series. Dorenbos[6] discussed the effect of the Coulomb and spin exchange interaction between the 5*d* electron and the 4*f* electrons on the ionization energy of divalent lathanide ions. He proposed, based on experimental data, that for the lighter lanthanide ions ($n < 7$) the Madelung energy term and the two exchange terms contribute equally but with an opposite sign to the ionization energy. As a result the lowest energy 5*d* states of the lighter lanthanide ions are predicted to be located at the same position relative to the CB.

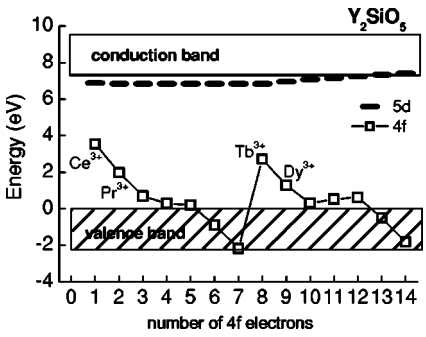

FIG. 6. Schematic of the energy level positions of the trivalent lanthanide ions in Y_2SiO_5 based on the temperature and spectrally resolved photocurrent excitation study presented in this work and the construction method described in Ref. 6.

It has to be noted that we have not established the precise location of the lowest energy 5*d* state of Pr^{3+} like we did for Ce^{3+}, since more than one combination of $\Delta E_1 - \Delta E_2$ is equal to 0.29 eV or 0.25 eV for YSO and LSO, respectively. The analysis of the experimental results, however, convincingly show that a $4f5d \rightarrow 4f^2$ intersystem crossing lowers the effective ionization barrier so that the lowest energy 5*d* state of Pr^{3+} can still be positioned at the same energy below the CB as Ce^{3+}. To pinpoint the lowest energy 5*d* state of Pr^{3+}, the intersystem-crossing activation energy ΔE_2 should be deduced, in a separate experiment, from the temperature dependence of the $4f^2 \rightarrow 4f^2$ and $4f5d \rightarrow 4f^2$ luminescence lifetime and intensity.

Figure 6 summarizes the data for Y_2SiO_5 in a schematic energy level scheme (a similar picture can be drawn for LSO). The scheme was constructed using the construction method as described in Ref. 6 with the photocurrent excitation data of Ce^{3+} as the point of reference to place the 5*d* state relative to the CB bottom. The energy of the bottom of the CB was taken 0.6 eV higher than the 6.8 eV energy for exciton creation measured in Ref. 16. 4*f* to 5*d* center of gravity transition energies for Pr^{3+} and Ce^{3+} used to place the ground states within the gap were taken from Refs. 13–16.

This schematic shows that the 5*d* states of Ce^{3+} and Pr^{3+} have about the same distance from the CB bottom but that the ground state of Pr^{3+} is located 1.5 eV deeper in the forbidden gap. When going through the lanthanide series the 4*f* ground state positions follow the free ion ionization energy. The 5*d* excited states remain at a constant position until Gd^{3+} and then move up into the CB. Figure 6 can be used as a guideline to predict ionization- or charge transfer energies of other Ln^{3+} ions as well as storage, thermoluminescence or long persistent afterglow properties in these hosts.

ACKNOWLEDGMENTS

This research was supported by a grant from the (US) National Science Foundation and the Dutch Technology Foundation (STW).

[1] C. Pedrini, F. Rogemond, and D. S. McClure, J. Appl. Phys. **59**, 1196 (1986).
[2] W. M. Yen, M. Raukas, S. A. Basun, W. van Schaik, and U. Happek, J. Lumin. **69**, 287 (1996).
[3] C. W. Thiel, H. Cruguel, H. Wu, Y. Sun, G. J. Lapeyre, R. L. Cone, R. W. Equall, and R. M. Macfarlane, Phys. Rev. B **64**, 085107 (2001).
[4] C. W. Thiel, Y. Sun, and R. L. Cone, J. Mod. Opt. **49**, 2399 (2002).
[5] P. Dorenbos, J. Lumin. **91**, 91 (2000).
[6] P. Dorenbos, J. Phys.: Condens. Matter **15**, 2645 (2003).
[7] P. Dorenbos, J. Phys.: Condens. Matter **15**, 8417 (2003).
[8] P. Dorenbos, J. Lumin. **108**, 301–305 (2004).
[9] E. van der Kolk, P. Dorenbos, J. T. M. de Haas, and C. W. E. van Eijk, Phys. Rev. B **71**, 045121 (2005).
[10] E. van der Kolk, S. A. Basun, G. F. Imbusch, and W. M. Yen, Appl. Phys. Lett. **83**, 1740 (2003).
[11] M. Raukas, S. A. Basun, W. van Schaik, W. M. Yen, and U. Happek, Appl. Phys. Lett. **69**, 3300 (1996).
[12] H. Suzuki, T. A. Tombrello, C. L. Melcher, and J. S. Schweitzer, Nucl. Instrum. Methods Phys. Res. A **320**, 263 (1992).
[13] P. Dorenbos, M. Marsman, C. W. E. van Eijk, M. V. Korzhik, and B. I. Minkov, Radiat. Eff. Defects Solids **135**, 325 (1995).
[14] J. Choi, S. A. Basun, L. Lu, W. M. Yen, and U. Happek, J. Lumin. **83–84**, 461 (1999).
[15] H. Suzuki, T. A. Tombrello, C. L. Melcher, and J. S. Schweitzer, Nucl. Instrum. Methods Phys. Res. A **320**, 263 (1992).
[16] V. Yu. Ivanov, V. L. Petrov, V. A. Pustovarov, B. V. Shulgin, V. V. Vorobjov, E. G. Zinevich, and E. I. Zinin, Nucl. Instrum. Methods Phys. Res. A **470**, 358 (2001).
[17] C. Pedrini, D. S. McClure, and C. H. Anderson, J. Chem. Phys. **70**, 4959 (1979).